minerals

MDPI

Article

Cu–S Isotopes of the Main Sulfides and Indicative Significance in the Qibaoshan Cu–Au Polymetallic Ore District, Wulian County, Shandong Province, North China Craton

Yuqin Sun [1], Xin Wang [2], Yan Zhang [1,*], Dapeng Li [1,*], Wei Shan [1], Ke Geng [1], Pengfei Wei [1], Qiang Liu [1], Wei Xie [1] and Naijie Chi [1]

[1] Key Laboratory of Gold Mineralization Processes and Resource Utilization, Ministry of Natural Resources, Shandong Provincial Key Laboratory of Metallogenic Geological Process and Resource Utilization, Shandong Institute of Geological Sciences, Jinan 250013, China; sunyuqin86@163.com (Y.S.)
[2] Number Eight Institute of Geology and Mineral Resources Exploration of Shandong Province, Rizhao 276826, China
* Correspondence: sddkyzy@163.com (Y.Z.); dpengli@126.com (D.L.)

Abstract: With a focus on the Cu isotope geochemistry of chalcopyrite, this paper analyzed the Cu isotope geochemistry of the Qibaoshan crypto-explosive breccia-type Cu–Au polymetallic ore district in Wulian, Shandong Province, North China Craton (NCC). Combined with the results of the in situ sulfur isotope analysis of sulfides, a certain reference and evidence for the study of the genetic mechanism of the epithermal-porphyry Cu polymetallic metallogenic system were provided. The results of the in situ isotope analysis show that the $\delta^{34}S$ values of the main sulfides in the Qibaoshan Cu–Au polymetallic ore district range from −6.81‰ to +3.82‰ and are likely to be attributed to the mixing of the derived mantle with the surrounding sedimentary rock assimilation. The ore-forming mechanism may be related to the progressive cooling and transition of the earliest hydrothermal fluids that were dominated by H_2S under relatively reducing conditions, followed by a gradual transition from oxidation to reduction. The Cu isotopic composition of the sulfides in ores ($\delta^{65}Cu$ = +0.169‰–+0.357‰) decreases with depth, which is likely caused by the upward transport of heavier Cu isotopes. The upper part of the crypto-explosive breccia pipe in the Qibaoshan area may be relatively more gaseous, resulting in the enrichment of $\delta^{65}Cu$. As the gas phase decreases and the liquid phase increases with depth, the $\delta^{65}Cu$ value gradually decreases. This indicates the transition from a low-temperature phyllic alteration to a high-temperature K-feldspar alteration. Large, concealed pluton intrusions or orebodies may be present at a depth of the Qibaoshan area. The heavy $\delta^{65}Cu$ characteristic is a potential indicator for tracing the fluid activity of the porphyry system and searching for Cu mines. The results provide a reference for the study of the genetic mechanisms of the epithermal-porphyry Cu polymetallic metallogenic system.

Keywords: Qibaoshan ore district; crypto-explosive breccia; Cu–Au polymetallic; Cu isotope; in situ sulfur isotope; concealed orebody

check for updates

Citation: Sun, Y.; Wang, X.; Zhang, Y.; Li, D.; Shan, W.; Geng, K.; Wei, P.; Liu, Q.; Xie, W.; Chi, N. Cu–S Isotopes of the Main Sulfides and Indicative Significance in the Qibaoshan Cu–Au Polymetallic Ore District, Wulian County, Shandong Province, North China Craton. *Minerals* **2023**, *13*, 723. https://doi.org/10.3390/min13060723

Academic Editors: António Manuel Nunes Mateus and David Lentz

Received: 15 March 2023
Revised: 22 May 2023
Accepted: 23 May 2023
Published: 25 May 2023

Copyright: © 2023 by the authors. Licensee MDPI, Basel, Switzerland. This article is an open access article distributed under the terms and conditions of the Creative Commons Attribution (CC BY) license (https://creativecommons.org/licenses/by/4.0/).

1. Introduction

With the advent of multi-collector inductively coupled plasma mass spectrometry (MC-ICP-MS), research on nontraditional stable isotopes have developed rapidly [1–9]. The theoretical system of Cu isotope geochemistry is essentially established [10–12]. Cu isotopes are widely used in ore deposits, including their potential to trace metallogenic temperatures and identify the metallogenic source and process [13,14]. Cu isotope studies have been carried out on magmatic deposits [15–17], collision and subduction-type porphyry Cu deposits [18–22], skarn-type Cu deposits [23], VMS (volcanic-associated massive sulfide)-type deposits [24,25], porphyry-hydrothermal vein-type Cu or Cu polymetallic

deposits [26–31], and sedimentary deposits [32,33]. The Cu isotope fractionation mechanisms under different conditions have also been developed [34–37]. In general, the variation range of the Cu isotopic composition in magmatic deposits is narrow and concentrated ~0‰. Compared with high-temperature magmatic deposits, the variation in Cu isotopes in skarn-porphyry and hydrothermal vein-type deposits is large. Chalcopyrite in low-temperature hydrothermal veins and sedimentary deposits is enriched in a light Cu isotope. The redox-driven Cu isotope fractionation can be used to distinguish different types of Cu deposits.

As a direct ore-forming element, the composition of Cu isotopes can facilitate the identification of ore-forming metal sources. Thus, Cu isotopes can be used to trace the source of metallogenic materials [38,39]. The Cu isotopic composition of the Cu-bearing minerals formed in different metallogenic stages is different, and the metallogenic process can be defined according to the Cu isotopic composition of Cu-bearing minerals [18,38,40]. In general, the δ^{65}Cu values of Cu-bearing minerals in porphyry Cu deposits are characterized by the following trend: leaching zone < plutonic primary ore zone < secondary enrichment oxidation zone [20,41]. This trend can play an indicative role in the deep exploration of Cu mines. Therefore, Cu isotope tracing technology is expected to provide clues to the sources of metallogenic materials, the division of metallogenic stages and the vertical zoning of Cu mineralization zones in different types of Cu deposits. Mason et al. [24] reported that the Cu isotopic composition of various sulfides in Russia's Alexandrinka volcanic massive sulfide (VMS) deposit is uniform. However, Zhu et al. [38] and Rouxel et al. [39] revealed the presence of significant isotopic fractionation in the Cu isotopic composition of sulfide in the submarine hydrothermal deposits, with a highly varying range of δ^{65}Cu values. The δ^{65}Cu value of Cu-bearing minerals from hypogene ores is ~0‰ [20,41–43]. Moreover, Cu isotopes also have great potential to explain the fluid pathway and metal precipitation mechanism in magmatic–hydrothermal systems [20,42–44].

The Qibaoshan Cu–Au polymetallic ore district, located in the eastern North China Craton (NCC), is an important crypto-explosive breccia-type Cu–Au deposit. It is genetically related to the hypabyssal magmatic intrusion and hydrothermal activity [45–48]. Previous analysis of the sulfide sulfur isotopes in the Qibaoshan Cu–Au polymetallic ore district via the single mineral powder reveals the deep crust to be the source of the ore sulfur [45–47]. However, sulfide contains other sulfide inclusions; thus, the sulfur isotope value obtained by the single mineral powder method cannot accurately represent the true value of the single sulfide mineral. This consequently affects the source tracing of sulfur and the identification of the metallogenic process. Therefore, the in situ sulfur isotope analysis of sulfides can better reflect the characteristics of ore-forming fluid [49–51]. Moreover, research on Cu isotopes in the Cu deposits associated with terrestrial volcanic–subvolcanic hydrothermal fluids is rare. The evolution of ore-forming fluids and the indicative significance of mineralization have not been limited, and the genesis of the Qibaoshan Cu–Au polymetallic ore district remains unclear.

In this paper, we report the Cu and the in situ sulfur isotopic analysis of the sulfides in the Qibaoshan crypto-explosive breccia-type Cu–Au deposit, tracing the source of the metallogenic materials and predicting deep mineralized alteration zones and hidden intrusions. Finally, the results obtained from the study can be used as a guide to evaluate the mineral prospecting potential in the Qibaoshan area.

2. Regional Geology

The study area is located at the intersection of the Jiaolai Basin and the eastern segment of the Tan-Lu Fault Zone (also known as the Yishu Fault Zone) in the eastern part of the NCC, northwest of the Wulian-Qingdao Fault Zone (F1). It is also adjacent to the Jiaonan uplift-Sulu ultrahigh-pressure metamorphic belt, whose spatial distribution is mainly controlled by the Yishu Fault Zone (Figure 1). The westward subduction of the Pacific plate during the Late Mesozoic triggered the reactivation of the regional NNE-trending Changyi-Dadian Fault (F2) and the Wulian-Qingdao Fault (F1), forming a series of volcanic–

subvolcanic magmatic activity zones. In general, the interior of the caldera is mainly occupied by intermediate–basic, intermediate–felsic and alkaline volcanic–intrusive complexes, providing favorable geological conditions for the formation of Cu–Au polymetallic deposits [46,47,52–54].

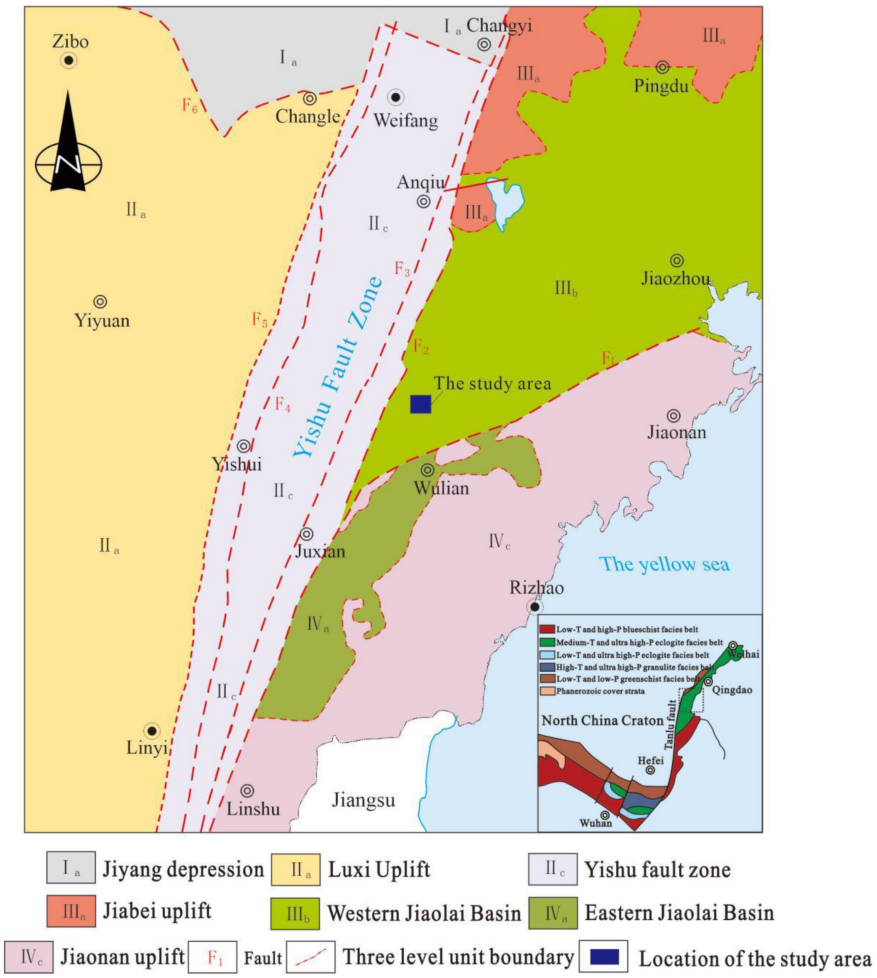


Figure 1. Regional tectonic map of the study area (modified from [55]).

By the tectonic recombination, the fault structure development can be divided into three groups according to the direction of its spatial distribution, including NE-trending, NNE-trending, and NW-trending structures, of which the largest are the NNE-trending Yishu Fault Zone (F2–F5) and the NE-trending Wulian-Qingdao Fault (F1) (Figure 1). The latter fault controls the formation of the Jiaolai Basin and the Yanshanian magmatic-volcanic activity. A few of the Cretaceous intermediate–felsic intrusions were exposed in the region, including granite, monzonite, syenite and diorite [46,56]. The outcropping stratigraphic units in the area are mainly the Bamudi Formation and Fanggezhuang Formation of the Qingshan Group from the Cretaceous of the Mesozoic, and the Shanqian Formation from the Quaternary is the secondary. The magmatic rocks in the area are mainly Mesozoic intermediate-acid rocks, such as the Qibaoshan intrusive complex, which are composed of intrusive rocks of different periods and lithologies. The outcropping area is ~25 km^2. The plane shape is a slightly longer ellipse in the NW-SE-trending, with long and short axes lengths of ~5.5 km and ~4.5 km, respectively (Figure 2). The mineral resources in the southern margin of the Jiaolai Basin, which includes the study area, are not widely developed. However, there are many types of Cu polymetallic deposits (mineralization points).

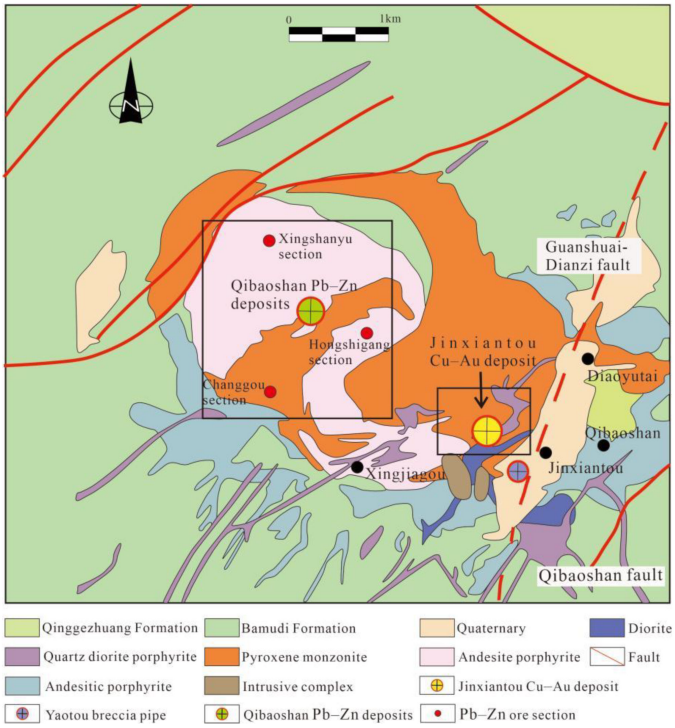


Figure 2. Regional geological map of the intrusive rock distribution in the Qibaoshan, Wulian County (modified from [56,57]).

3. Ore Deposit Geology

The Qibaoshan Cu–Au polymetallic ore district in Wulian, Shandong Province, is a typical crypto-explosive breccia genetically with epithermal subvolcanic hydrothermal fluid [48]. Three typical deposits are located in the Qibaoshan area, including the Jinxiantou Cu–Au deposit, the Qibaoshan Pb–Zn deposit and the Diaoyutai pyritic deposit (Figure 2). Among them, the Jinxiantou Cu–Au deposit is located in the south of the study area, which mainly develops crypto-explosive breccia-type, veinlet-disseminated-type and shattered-altered rock-type mineralization. The orebodies generally occur in the crypto-explosive breccia pipe of the Qibaoshan complex, and the ore host surrounding the rocks are mainly granodiorite porphyrite (quartz diorite porphyrite), diorite and andesite porphyrite. The Qibaoshan Pb–Zn deposit is dominated by vein-type mineralization, which comprises the Changgou, Hongshigang and Xingshanyu sections [46]. The mineralization types are mainly quartz–calcite veins and structural altered rock types. The Diaoyutai pyritic deposit is characterized by layer-like and layer pyritization. The Number Eight Institute of Geology and Mineral Resources Exploration of Shandong Province recently discovered the Yaotou ore-bearing crypto-explosive breccia pipe 600 m southeast of the Jinxiantou breccia pipe. In addition, seven new Pb–Zn–Cu–Au–Ag polymetallic orebodies have been newly discovered using the 2020ZK1 drill hole in the Yaotou area. The two-dimensional seismic profile reveals that the breccia pipe extends 1200 m deep along the southeastern structural channel. Typical fracturing breccia and burst breccia are developed in the breccia pipe, and phyllic alteration, silicification, carbonation and K-feldspathization are significant. The breccia pipe contains the Cu–Ag orebody associated with the No.1 Pb–Zn ore deposit, and the No.2 Pb–Zn–Cu–Ag is associated with the orebody. The accumulative plumb thickness of the Pb–Zn polymetallic orebody is 14.15 m. There are many differences among the deposits in terms of the mineralization types, ore characteristics, ore-forming element combinations and surrounding rock alteration characteristics. This study mainly focuses on the Jinxiantou Cu–Au deposit and Yaotou breccia pipe, which both belong to the Qibaoshan Cu–Au polymetallic ore district.

Based on the lithology, contact relation and zircon LA-ICP-MS dating results of magmatic rocks in the Qibaoshan area, the magmatic-volcanic activity system can be divided into four periods: pyroxene diorite stage (the age of 174.8 ± 1.7 Ma, dated by zircon U-Pb); Qingshan Group volcanic stage (the age of 133.8 ± 1.8 Ma, dated by zircon U-Pb); pyroxene andesite porphyrite-amphibolic andesite porphyrite and granodiorite porphyry-quartz diorite porphyrite stage (the age of 129.6 ± 1.2 Ma, dated by zircon U-Pb); and andesitic porphyrite-diorite porphyrite stage (the age of 111.5 ± 1.2 Ma, dated by zircon U-Pb) [46]. Cu–Au mineralization is closely related to the granodiorite porphyry in space, and Pb–Zn mineralization is related to the hypabyssal intrusive activity of the andesitic porphyrite. The dominant mineralization type is the crypto-explosive breccia, and the structurally altered rock type and veinlet-disseminated type are developed in local areas (Figure 3). The industrial ore type is the low-S Cu-bearing ore, and the main metal mineral is specularite, followed by chalcopyrite, pyrite and galena, which are distributed below the oxidation zone. The natural ore type belongs to the primary Cu-bearing ore (Figure 3a,b). A small amount of oxidized ore is present near the surface, and secondary enrichment cannot be observed. Figure 3 presents the typical characteristics of the ore fabric, with crystalline granular, crushing, interstitial and metasomatic textures. Moreover, ore structures are characterized by breccia (Figure 3c–e), fine vein and fine vein-disseminated structures (Figure 3f–h). The breccia structure is the main ore type and comprises quartz diorite porphyrite and pyroxene diorite porphyrite, with a small amount of pyrite, carbonate, chalcedonic quartz and opal, and the types of cement are chalcedonic quartz, pyrite and calcite veins.



Figure 3. The main ore composition and structure characteristics of Qibaoshan Cu–Au polymetallic ore district. (**a**) Jinxiantou sericite-silicified altered rock ore containing chalcopyrite, tetrahedrite, covellite and other minerals. (**b**) Jinxiantou carbonated-altered rock ore containing chalcopyrite, pyrite, specularite, siderite and other minerals. (**c**) Jinxiantou volcanic breccia ore containing chalcopyrite, pyrite, siderite and other minerals; the breccia and its margins are often altered by carbonate. (**d**) Weakly silicified, baritized, and carbonated-altered rock ore in the Hongshigang section, in which quartz–carbonate vein cuts can be observed. (**e**) Veinlet-disseminated altered rock ore. (**f**) Veinlet galena in granodiorite.

The rock alteration related to the Cu–Au deposits mainly includes beresitization, silicification, sericitization, K-feldspathization, chloritization, carbonation and kaolinitization. In particular, the alteration types closely related to mineralization are silicification and K-feldspathization. Altered rock is an important indicator of prospecting (Figure 3a,b,f,g).

Beresitization is the key alteration type in the early ore-forming period. Furthermore, silification and K-feldspathization can be employed as alteration markers of ore-bearing breccia.

Based on the mineral assemblage and mineral symbiotic characteristics (Figure 4), the mineralization of the Qibaoshan Cu–Au polymetallic ore district can be divided into six metallogenic stages: pyrite–quartz stage; chalcopyrite–chalcocite–bornite–pyrite–quartz stage; specularite–pyrite–chalcopyrite–quartz–carbonate stage; quartz–polymetallic–sulfide stage; chalcopyrite–pyrite–quartz stage; and late carbonate stage.

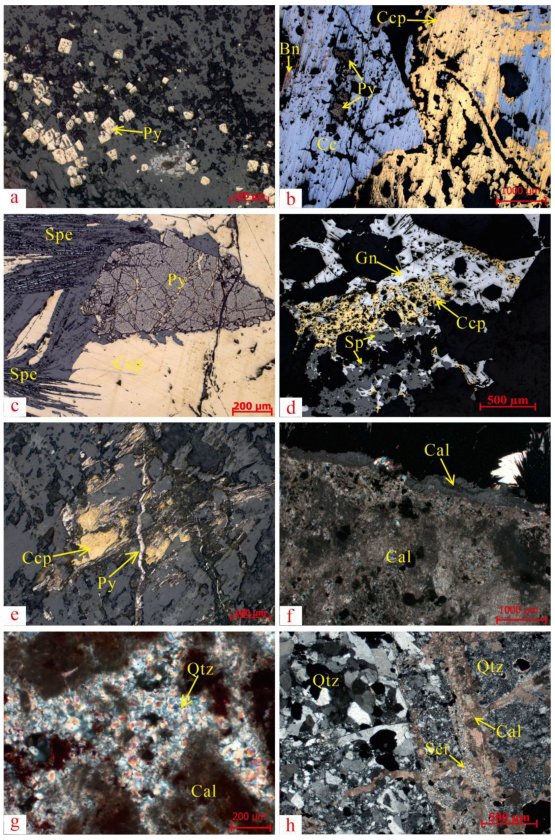


Figure 4. Photomicrographs of the Qibaoshan Cu–Au polymetallic ore district. (The study mainly selected sulfides from the early specularite–pyrite–chalcopyrite–quartz–carbonate stage and the late chalcopyrite–pyrite–quartz stage for analysis). (**a**) Pyrite–quartz stage: pyrite is distributed in semi-automorphic granular form (reflected light). (**b**) Chalcopyrite–chalcocite–bornite–pyrite–quartz stage: chalcopyrite fills along the interstices of chalcocite, and bornite solid solution and pyrite inclusions can be seen within chalcocite (reflected light). (**c**) Specularite–pyrite–chalcopyrite–quartz–carbonate stage: early pyrite and specularite are altered by chalcopyrite (reflected light). (**d**) Quartz–polymetallic–sulfide stage: galena, chalcopyrite and sphalerite are coeval (reflected light). (**e**) Chalcopyrite–pyrite–quartz stage: pyrite is finely veined, and chalcopyrite and pyrite are coeval (reflected light). (**f**) Carbonate stage: two phases of carbonate are visible (transmitted cross-polarized light). (**g**) Silicification and carbonation (transmitted cross-polarized light). (**h**) Multi-stage silicification and late fractures filled with carbonate minerals and sericite (transmitted cross-polarized light). Py—pyrite, Ccp—chalcopyrite, Cc—chalcocite, Bn—bornite, Spe—specularite, Gn—galena, Sp—sphalerite, Qtz—quartz, Ser—sericite, Cal—calcite.

4. Samples and Analytical Methods

4.1. Samples

The study selected typical orebodies and strata to collect wallrock and ore samples, and they were collected from different depths of the drill hole. The chalcopyrite and pyrite samples used for the Cu and S isotopes were taken from the Jinxiantou open pit,

Hongshigang Pb–Zn section (Figure 2) and the drill hole (QBS2020ZK1) of Yaotou crypto-explosive breccia pipe (Figure 5).

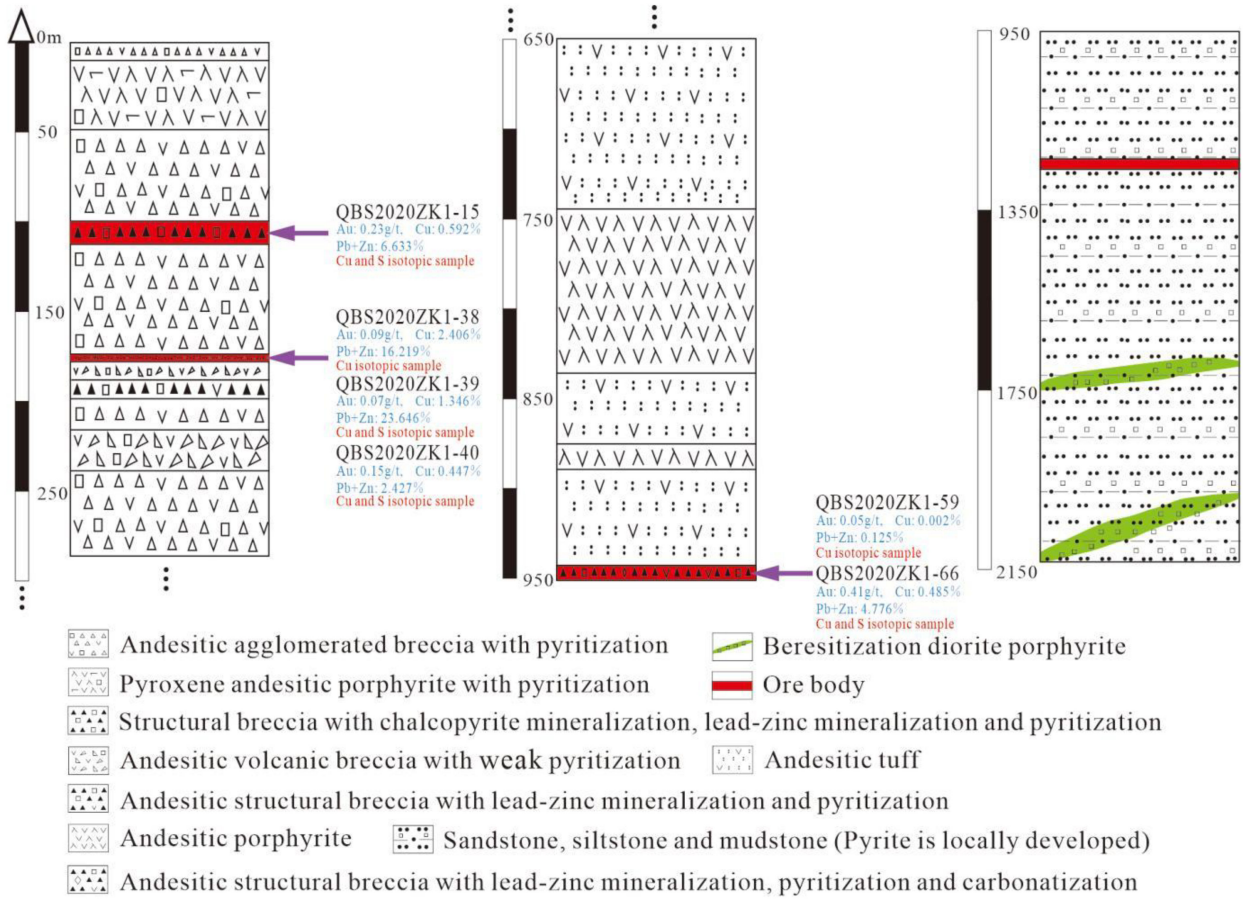


Figure 5. A section of the lithological section from the QBS2020ZK1 drill hole at the Yaotou crypto-explosive breccia pipe (modified from [58]).

The Cu isotope analysis of chalcopyrite and the in situ sulfur isotope analysis of pyrite and chalcopyrite were performed at the State Key Laboratory of Isotope Geochemistry, Guangzhou Institute of Geochemistry, within the Chinese Academy of Sciences.

4.2. Copper Isotope Analysis

The detailed procedures for sample digestion, column chemistry and instrumental analysis in this study follow the established methods [59–61] modified from Maréchal et al. [62]. Only a brief description is provided here.

The sample powders were weighed based on their known Cu concentrations and then digested in the sub-boiling distillation of concentrated HCl+HNO_3+HF. Samples containing approximately 1 μg Cu were accurately weighed and transferred to a 1 mL PFA solution tank, dissolved at 140 °C for 48 h with 1 mL HNO_3 and 2 mL HF, and subsequently dried at 120 °C. The chemical purification of Cu is based on the process of Maréchal et al. [62]. Purification was performed with a 2 mL anion exchange resin (Bio-Rad, AG MP-1, 100–200 mesh) and, again, with a 1 mL anion exchange resin (Bio-Rad, AG MP-1, 100–200 mesh). The received solution was dried at 120 °C, and several drops of nitric acid were added to remove any possible organic matter residue and then subsequently extracted with 2 mL of 2% (m/m) HNO_3.

Cu isotope ratios were determined using the Neptune Plus MC-ICP-MS from Thermo Fisher Scientific in Germany. The sample-standard bracketing method was used to correct instrumental mass fractionation and drifting. The sensitivity of the ^{63}Cu instrument

is approximately 35 V/(μg/g) with the combination of a jet sampling cone and an H intercepting cone. The Cu concentration is 200 ng/g, and the accuracy exceeds 0.1‰. Copper isotope data are reported in standard δ-notation in per mil, relative to the standard reference material:

$$\delta^{65}Cu = ((\delta^{65}Cu/\delta^{63}Cu)_{sample}/(\delta^{65}Cu/\delta^{63}Cu)_{NIST\ 976} - 1) \times 1000$$

4.3. Sulfur Isotope Analysis

The sulfur isotopic compositions of sulfides were measured using a Neptune Plus MC-ICP-MS (Thermo Fisher Scientific, Germany) equipped with a Resolution S155 193 nm laser and ablation, using helium as the carrier gas. Three reference materials, IAEA-S3, GBW04414 and GBW04415, were used for the analysis and calibration, and the analysis accuracy exceeds 0.2‰. Instrument operating conditions and analytical methods are the same as those described by Fu et al. [63]. The single spot ablation mode was used together with a spot size of 22 μm and a pulse frequency of 6 Hz. The laser energy density was fixed at 4.0 J/cm^2. ^{32}S and ^{34}S signals were received by the Faraday cups simultaneously. A total of 200 sets of data were collected, and the total time was approximately 27 s. The instrument parameters were adjusted with the sulfide standard samples HN, JX and ZX to ensure that they were in their optimal state. In order to reduce the influence of the matrix effect on the testing results, sulfides similar to the sample matrix were used as the standard samples in the analytical process, and the SSB method was used for quality discrimination correction.

5. Results

5.1. Copper Isotopes in Chalcopyrite

The lithologies, sampling locations and chalcopyrite isotope analyses for 11 samples are summarized in Table 1. The δ^{65}Cu values of all samples vary from +0.076‰ to +0.357‰, with a varied range of 0.281‰, which is typical of the mineralized systems with ~0‰ δ^{65}Cu values that have not been influenced by low-temperature redox processes [20]. The sample from the biotite diorite (wallrock) has a more depleted Cu isotope composition (+0.076‰) than those from the ores (0.169‰~+0.357‰). The δ^{65}Cu value range of the Jinxiantou deposit, the Hongshigang section and the top of the Yaotou breccia pipe is very small (+0.223~+0.357‰). However, the δ^{65}Cu values of chalcopyrite tend to decrease with the depth of the Yaotou breccia pipe. The δ^{65}Cu values of the two chalcopyrite samples are 0.284‰ and 0.169‰, with elevations of -808 m and -814 m, respectively.

The δ^{65}Cu values of the chalcopyrite of the ore have a range of +0.169‰~+0.357‰, with an average of+0.265‰, which is consistent with the δ^{65}Cu value (0.30‰) [64] of chalcopyrite in porphyry Cu–Au deposits.

Table 1. Cu isotopic data of chalcopyrite from the Qibaoshan Cu–Au polymetallic ore district.

No.	Sample Number	Sample Lithology	Sampling Position and Elevation	δ^{65}Cu (‰)	2SD
1	QBS-1	Biotite diorite (wallrock)		0.076	0.009
2	QBS-3	Carbonated-altered rock	Jinxiantou +10 m	0.239	0.011
3	QBS-4	Sericite-silicified altered rock		0.223	0.013
4	QBS-7	Volcanic breccia-type altered rock		0.250	0.055
5	QBS-17	Silicified-carbonated altered rock	Hongshigang +112 m	0.252	0.035
6	QBS2020ZK1-15	Sericite-silicified structural breccia	Yaotou +24 m	0.357	0.019
7	QBS2020ZK1-38	Sulfide-bearing altered rock	Yaotou −43 m	0.279	0.027
8	QBS2020ZK1-39	Sulfide-bearing sericite-silicified structural breccia	Yaotou −43 m	0.318	0.040
9	QBS2020ZK1-40	Carbonated-altered rock	Yaotou −44 m	0.279	0.041
10	QBS2020ZK1-59	Carbonated-silicified altered rock	Yaotou −808 m	0.284	0.026
11	QBS2020ZK1-66	Sericite-silicified altered rock	Yaotou −814 m	0.169	0.015
		Average value of δ^{65}Cu		0.265	

Sample 1 is biotite diorite, not ore, and thus it is not included in the calculation of the mean.

5.2. In Situ Sulfur Isotopes in Sulfides

The S isotopes of the sulfides are shown in Table 2 and Figures 6 and 7. The overall δ^{34}S values show a markedly spreading from −6.81‰ to +3.82‰ (n = 15). The chalcopyrite in the wallrock biotite diorite exhibits the lowest δ^{34}S values, with an average of −4.92‰ (n = 2). Chalcopyrite and pyrite in the altered breccia ores have δ^{34}S values ranging from −2.07‰ to +3.82‰ (n = 11) and −1.65‰ to +2.71‰ (n = 4), respectively.

The δ^{34}S values gradually decrease from the early stage (+3.26‰ to +3.82‰) to the late stage (−2.07‰ to +2.72‰) of mineralization. In general, The δ^{34}S values of pyrite are higher than those of paragenetic chalcopyrite.

Table 2. In situ sulfur isotopic data of metal sulfides from the Qibaoshan Cu–Au polymetallic ore district.

No.	Sample Number	Sample Lithology	Sampling Position and Elevation	Sulfide	δ34SV-CDT (‰)	Average
1	QBS-1	Biotite diorite	Jinxiantou +10 m	Chalcopyrite	−6.81	−4.92
2				Chalcopyrite	−3.03	(n = 2)
3	QBS-3	Carbonated-altered rock		Chalcopyrite	3.26	3.52
4				Chalcopyrite	3.78	(n = 2)
5	QBS-4	Sericite-silicified altered rock		Chalcopyrite	3.82	3.71
6				Chalcopyrite	3.61	(n = 2)
7	QBS-17	Silicified-carbonated altered rock	Hongshigang +112 m	Chalcopyrite	1.81	1.67
8				Chalcopyrite	1.52	(n = 2)
9	QBS2020ZK1-15	Sericite-silicified structural breccia rock	Yaotou +24 m	Pyrite	2.71	2.67
10				Pyrite	2.63	(n = 2)
11	QBS2020ZK1-39	Sulfide-bearing sericite-silicified structural breccia rock	Yaotou −43 m	Pyrite	1.35	1.35
12				Chalcopyrite	−1.57	−1.57
13	QBS2020ZK1-40	Carbonated-altered rock	Yaotou −44 m	Chalcopyrite	−2.07	−2.07
14	QBS2020ZK1-66	Sericite-silicified altered rock	Yaotou −814 m	Chalcopyrite	−1.95	−1.95
15				Pyrite	−1.65	−1.65

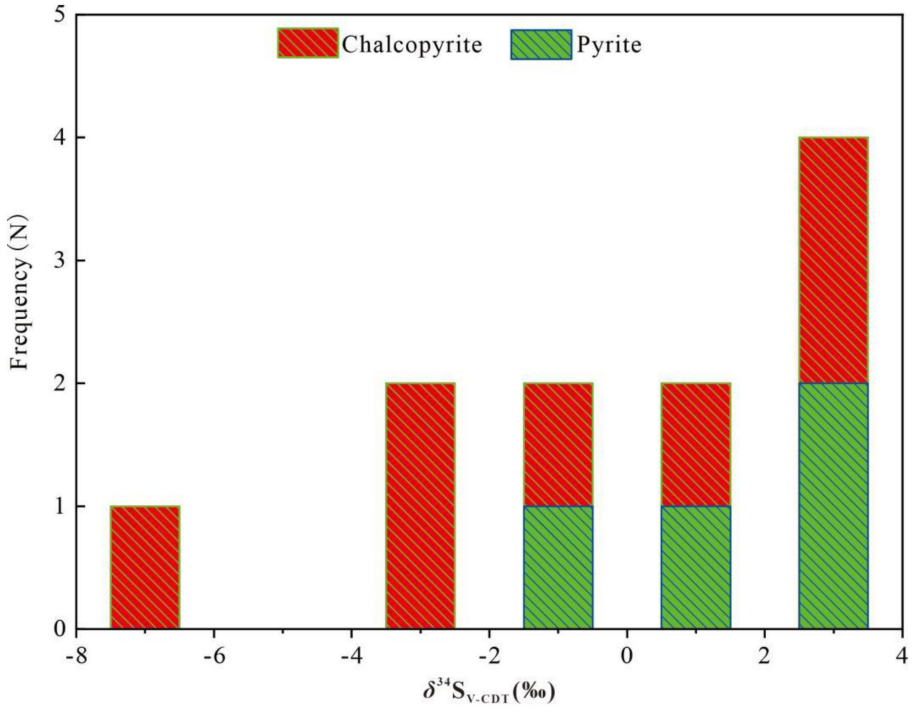


Figure 6. Histogram of in situ sulfur isotopic data of metal sulfides from the Qibaoshan Cu–Au polymetallic ore district.

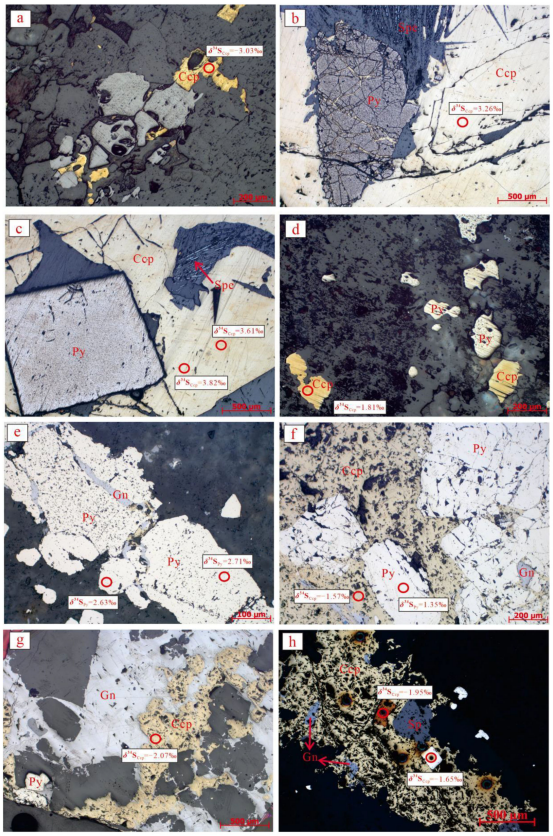


Figure 7. Reflected light photomicrographs showing the distribution of in situ sulfur isotopic characteristics of the main sulfides in the Qibaoshan Cu–Au polymetallic ore district. Ccp—chalcopyrite, Gn—galena, Py—pyrite, Spe—specularite, Sp—sphalerite. (**a**) QBS-1. (**b**) QBS-3. (**c**) QBS-4. (**d**) QBS-17. (**e**) QBS2020ZK1-15. (**f**) QBS2020ZK1-39. (**g**) QBS2020ZK1-40. (**h**) QBS2020ZK1-66. (**a**) is the wallrock biotite diorite; (**b**,**c**) represents the early stage of mineralization; (**d**–**h**) represents the late stage of mineralization.

6. Discussion

6.1. Cu Isotopic Variation in Chalcopyrite and Its Implications

Cu isotope studies may provide a mechanism for tracing the spatial and temporal distribution of Cu migration and precipitation in magmatic-hydrothermal ore deposits [18,42,65].

The δ^{65}Cu values of chalcopyrite in the Qibaoshan region analyzed in this study (+0.076 to +0.357‰) are typical of the Cu isotopic signatures of primary sulfides in magmatic-hydrothermal ore deposits, which have narrow ranges of δ^{65}Cu values (−1 to +1‰) [20], reflecting the origin of primary sulfides. In general, the δ^{65}Cu values of chalcopyrite in the wallrock are significantly lower than those of chalcopyrite in altered rock-type ore (Figure 8).

Among the ore samples collected at a similar elevation (Figure 9), the δ^{65}Cu value of chalcopyrite in the altered rocks in the crypto-explosive breccia pipe of the Yaotou area is significantly lower than that of the corresponding ores of the Jinxiantou deposit and Hongshigang section. There is a decreasing trend in the chalcopyrite δ^{65}Cu value towards the deep of the breccia pipe. This is consistent with the variation trend of sulfide from the Pebble porphyry-type Cu–Au-Mo deposit in Alaska [65] but opposite to that of sulfide from the high sulfidation epithermal-porphyry Cu–Au deposits of Tiegelongnan in Tibet [64]. In the Zijinshan epithermal Cu–Au deposit in China, there is controversy over the trend of δ^{65}Cu values with depth [44,66]. In a study investigating the Cu isotope of sulfide from the Northparkes porphyry-type deposit in Australia at different depths and alteration stages, Li et al. [67] revealed that the δ^{65}Cu value decreased from 0.2‰ to −0.4‰ from the mineralized core to the edge of the orebody, and subsequently rises to 0.8‰

to the peripheral propylitic surrounding rock. The authors attributed this to the isotope fractionation equilibrium between different phases. During the magma boiling process, the gas and liquid phases separate, heavy isotopes enter the gas phase, and light isotopes are enriched in the liquid phase [37]. The gas phase diffuses into the surrounding rock, and the liquid phase moves outward and subsequently precipitates as the temperature decreases. Therefore, the upper part of the crypto-explosive breccia pipe may be relatively rich in the gas phase, and the δ^{65}Cu value is enriched. As the gas phase decreases and the liquid phase increases with depth, the δ^{65}Cu value is reduced. The gradual reduction of the chalcopyrite δ^{65}Cu value with depth may indicate the existence of concealed pluton or orebodies at depth [68].

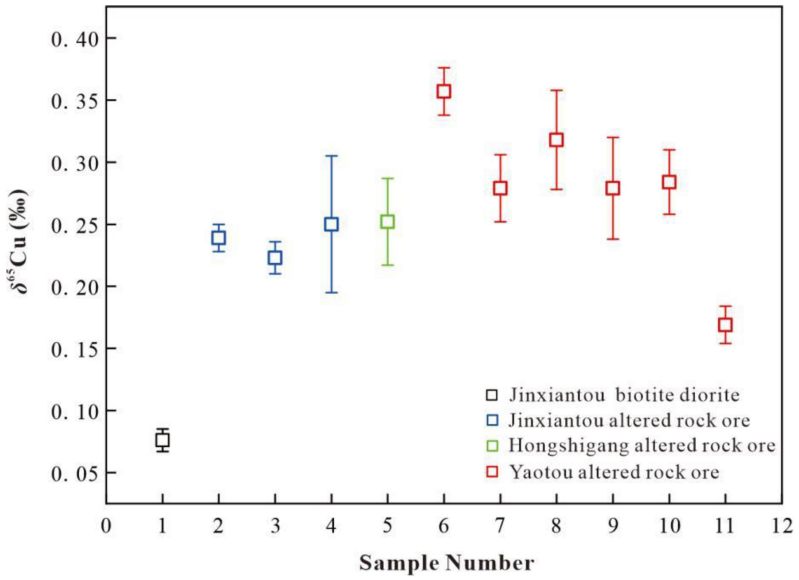


Figure 8. Distribution of the Cu isotopic composition of chalcopyrite in the Qibaoshan Cu–Au polymetallic ore district.

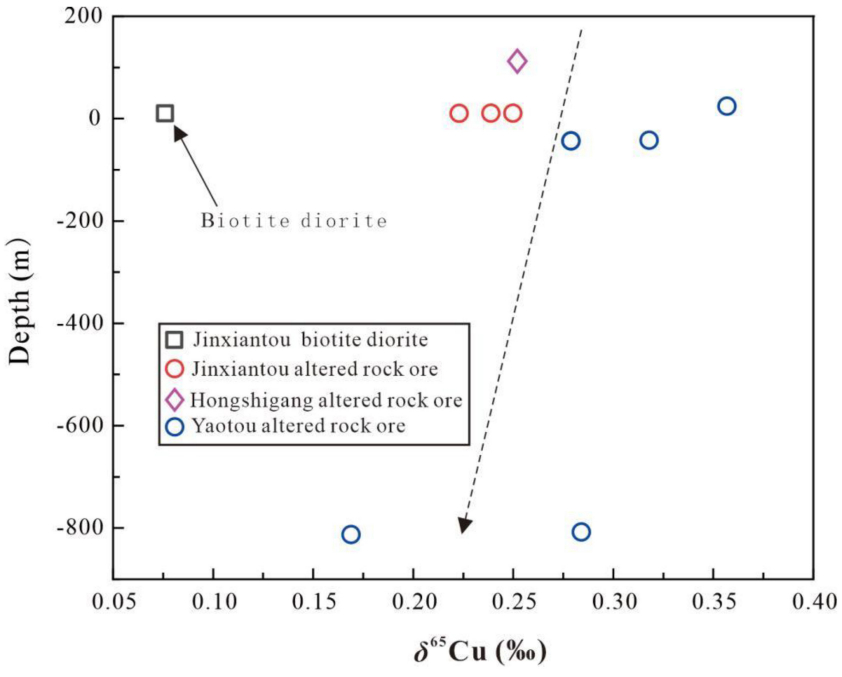


Figure 9. Relationship between the chalcopyrite Cu isotope and depth in the Qibaoshan Cu–Au polymetallic ore district.

The Cu isotopic fractionation mechanism in the mineralization process of epithermal Cu–Au deposits is key for exploring deep orebodies. Figure 10 reveals the Cu isotopic composition of chalcopyrite in the Qibaoshan Cu–Au deposit to be consistent with that of the porphyry-type Cu deposits worldwide. Previous studies have demonstrated the close relationship between the Cu isotope composition of sulfide in porphyry deposits and the alteration type of silicates. The δ^{65}Cu values of sulfides in different alteration zones exhibit differences. More specifically, the sulfide in the phyllic alteration zone, formed at low temperatures, generally has a positive δ^{65}Cu value, while that in the high-temperature potassic zone has a negative δ^{65}Cu value. This difference can be attributed to the Cu isotope fractionation of S in the different magmatic-hydrothermal fluid stages [65]. In the silicate system and multiphase coexisting partially melted silicate system, all the metal isotopes exhibit the Soret effect; that is, heavy isotopes are preferentially enriched at the low-temperature end, while light isotopes are enriched at the high-temperature end [69,70]. Therefore, the δ^{65}Cu of chalcopyrite in the Qibaoshan gradually decreases with the depth. This may indicate the transition from a low-temperature phyllic alteration to a high-temperature potassic alteration. The change in the chalcopyrite δ^{65}Cu value resulted in the Cu isotope fractionation between the magmatic fluid and precipitating sulfides due to variations in the pH and the cooling of magmatic-hydrothermal fluids along the fluid pathway [71].

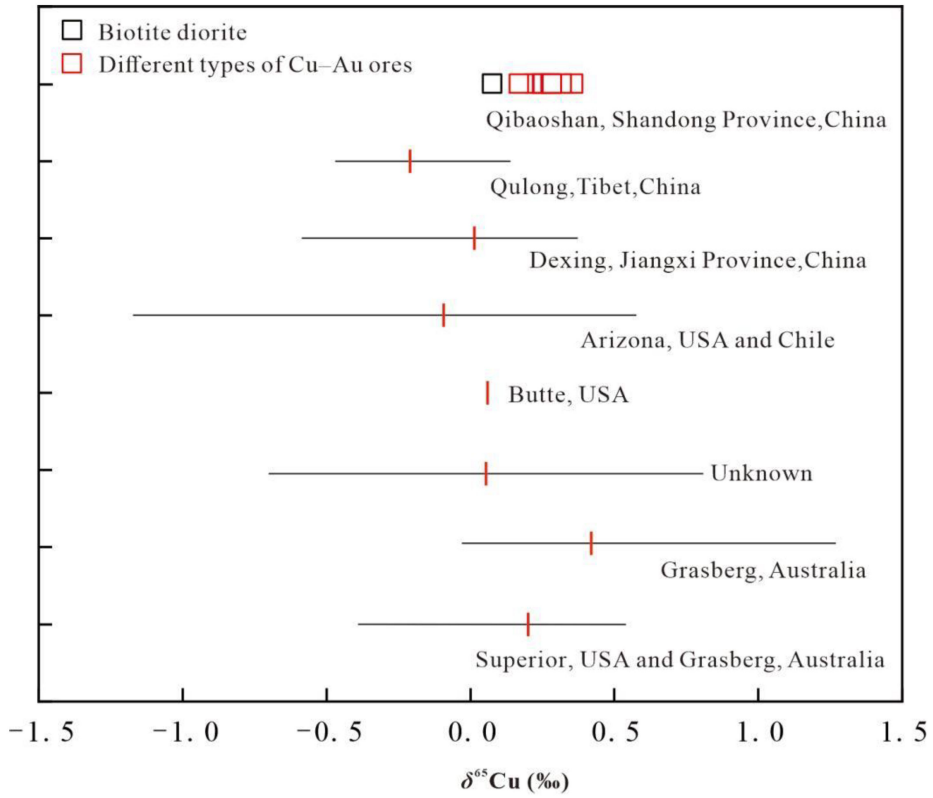


Figure 10. Cu isotopic composition of chalcopyrite in major porphyry-type Cu deposits in the world. (Data from [10] and references therein).

6.2. Sulfur Source

Wang [45] revealed that the range of sulfur isotope values of pyrite, chalcopyrite, galena and sphalerite in ores is +0.3‰~+5.1‰, with an average value of +3.16‰. Moreover, the sulfur isotope composition follows a tower distribution. Yu [46] determined the δ^{34}S values of 4 pyrite samples from the Jinxiantou deposit to range from +2.1‰ to +4.8‰, with an average value of +3.33‰. The δ^{34}S values of chalcopyrite samples are higher than those of pyrite, and the δ^{34}S values of the three chalcopyrite samples range from +4.8‰ to

+6.1‰, with an average of +5.4‰. The $\delta^{34}S$ value of Jinxiantou deposit ores also exhibits the characteristics of a tower distribution, indicating a single source for the ore sulfur. The $\delta^{34}S$ values of the three chalcopyrite samples from the Changgou section are all lower than that of the chalcopyrite from the Jinxiantou deposit, with a range of +3.3 to +4.2‰. The $\delta^{34}S$ values of the two galena samples in the Hongshigang section are +0.6‰ and +3.0‰, with an average value of +1.8‰. They concluded that $\delta^{34}S_{pyrite}$ is lower than $\delta^{34}S_{chalcopyrite}$ and indicated that the sulfur isotopes of pyrite and chalcopyrite had not reached the equilibrium fractionation in the metallogenic system of the Jinxiantou Cu–Au deposit [46]. However, they did not consider the differences in mineral assemblage and S isotope at different metallogenic stages.

In this study, we observed the chalcopyrite to exhibit the highest $\delta^{34}S$ value in altered rocks and the lowest in biotite diorite in the Jinxiantou open pit. The $\delta^{34}S$ values of sulfides from the mineralization in the Qibaoshan region exhibit a relatively wide range in $\delta^{34}S$ (-6.81 to +3.82‰), consistent with the magmatic origin for sulfur. The $\delta^{34}S$ of pyrite exceeds that of chalcopyrite in the Yaotou crypto-explosive breccia pipe, and the $\delta^{34}S$ value at depth is lower than that in the shallow (Figure 11). The $\delta^{34}S$ values of the altered rock in the Jinxiantou open pit and the upper area of the Yaotou breccia pipe are around 0‰. This indicates that the ore sulfur isotope belongs to the deep-source sulfur origin, and both Cu and Au mineralization are related to the deep-source magmatic activity.

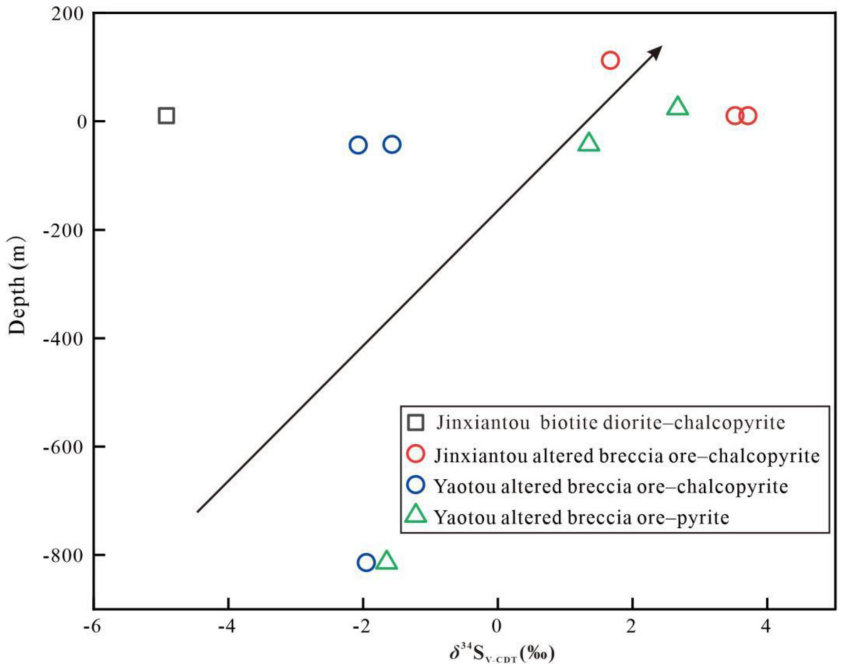


Figure 11. Correlation between the sulfur isotopes of the main sulfides and elevation at the Qibaoshan Cu–Au polymetallic ore district.

The sulfur isotopic composition can be employed to determine the evolution of ore-forming fluid and sulfur sources. Simple paragenetic associations of ore minerals that do not contain sulfate indicate speciation—that sulfur in ore-forming hydrothermal fluid migrates mainly in the form of S^{2-} and HS^{-} [72]. Based on previous detailed petrographic observations and other comprehensive identification approaches, chalcopyrite and pyrite in the main mineralization stage were selected for the subsequent analysis. The $\delta^{34}S$ value of chalcopyrite in the biotite diorite is -3.03‰ (Figure 7a), indicating the mixing characteristics of fluid and wallrock before mineralization. With the gradual evolution of ore-forming fluid, the early fluid is in an acidic oxidation state, accompanied by the precipitation of minerals such as specularite (Figure 7b,c), and the corresponding $\delta^{34}S$ value of chalcopyrite is positive. In the late stage, the ore-forming fluid gradually reduced, and sulfides such as

pyrite, chalcopyrite and sphalerite were precipitated (Figure 7d–h), and the $\delta^{34}S$ value of the corresponding sulfides gradually became negative. The S isotopic compositions of the paragenetic chalcopyrite and pyrite (Figure 7f) exhibit the trend $\delta^{34}S_{pyrite} > \delta^{34}S_{chalcopyrite}$. This is consistent with the high-temperature porphyry environments, which tend to record the equilibrium sulfur isotope fractionation principle [73,74].

As mentioned above, sulfides from the shallow part of the crypto-explosive breccia pipe are enriched in $\delta^{34}S$ compared to the deep section. Negative sulfur isotope values may be a result of the interaction between the fluid and surrounding rock [75] or the oxidation of ore-forming fluids [76]. However, the $\delta^{34}S$ value of the chalcopyrites associated with the oxidizing minerals, such as specularite and hematite, in the early stage of mineralization is positive. Therefore, it is not possible to directly determine the sulfur source via sulfur isotope analysis. The oxygen fugacity is high in the Cu–Au mineralization stage for the early mineralization of the Jinxiantou deposit, yet the $\delta^{34}S$ value of chalcopyrite is positive. Moreover, the oxygen fugacity decreases in the Pb–Zn mineralization stage for the late mineralization of the Yaotou area, yet the $\delta^{34}S$ values of chalcopyrite and pyrite are low (mostly negative). This is similar to the negative $\delta^{34}S$ value of chalcopyrite in biotite diorite. The sedimentary rocks, such as pyrite-bearing sandstone and mudstone (Figure 5), developed in the depth of the QBS2020ZK1 drill hole in the Yaotou area imply that the low $\delta^{34}S$ value of sulfide is the result of the interaction between the late low-temperature hydrothermal fluid and the surrounding rock. The presence of large quantities of specularite and sulfates, such as barite and gypsum, at Qibaoshan, however, may suggest that the fluid attained more oxidized conditions locally. The synsedimentary-diagenetic sulfides are the most probable source of sulfur in the gold deposits of the Ashanti Belt in Ghana [77]. The isotopically light sulfides could have been derived either from bacterial sulfate reduction (BSR) at the depositional site or pre-existing bacteriogenic pyrite in the sediments remobilized by the hydrothermal fluids [78]. Thus, the sulfur of sulfides in the Qibaoshan Cu–Au polymetallic ore district is likely to be attributed to the mixing of the mantle sulfur at depth and the sedimentary sulfur in the surrounding sedimentary rocks. The local oxidation of fluids may lead to the slightly negative $\delta^{34}S$ values of the sulfides.

Figure 12 reveals the $\delta^{34}S$ values to be consistent with the corresponding ranges of the NCC. The $\delta^{34}S$ values exhibit extensive variations with large negative values. The $\delta^{34}S$ values of biotite diorite fall within the range of volcanic H_2S, and the $\delta^{34}S$ values of altered rocks and breccia pipes vary greatly. Therefore, the ore-forming mechanism may be related to the progressive cooling and transition of the hydrothermal fluids that were dominated by H_2S under relatively reducing conditions [71]. Moreover, the $\delta^{34}S$ values of sulfide in the Yaotou area gradually become negative with depth. These results indicate that the sulfur in the Qibaoshan may have been characteristic of multiple sources, and the ore-forming fluids have experienced a long migration process. The Jinxiantou Cu–Au deposit is spatially related to granodiorite porphyry, and thus the Cu and Au mineralization time of the Jinxiantou deposit is slightly later than 125 Ma. The Pb–Zn mineralization in the Hongshigang deposit is closely related (spatially) to andesitic porphyrite, and the mineralization time is slightly later than 112 Ma [46].

6.3. Implication for Ore-Forming Process

In general, the fluid exsolved from the silicate magma in the porphyry deposits exhibits heavy $\delta^{65}Cu$ values (>0‰). As the fluid continues to evolve and inflows into the shallow layers, the single-phase fluid separates into brine- and gas-phase fluids. Compared with the parental silicate magma in the intrusions, different types of fluids have characteristics of relatively high $\delta^{65}Cu$ values [37]. During the evolution of the aforementioned metallogenic stages, the $\delta^{65}Cu$ and $\delta^{34}S$ values of the hydrothermal fluids increase gradually with the fluid's evolution (Figure 13). Therefore, the characteristic of high $\delta^{65}Cu$ is a potential indicator for fluid activity in the porphyry system and can be employed to search for enriched Cu deposits [37].

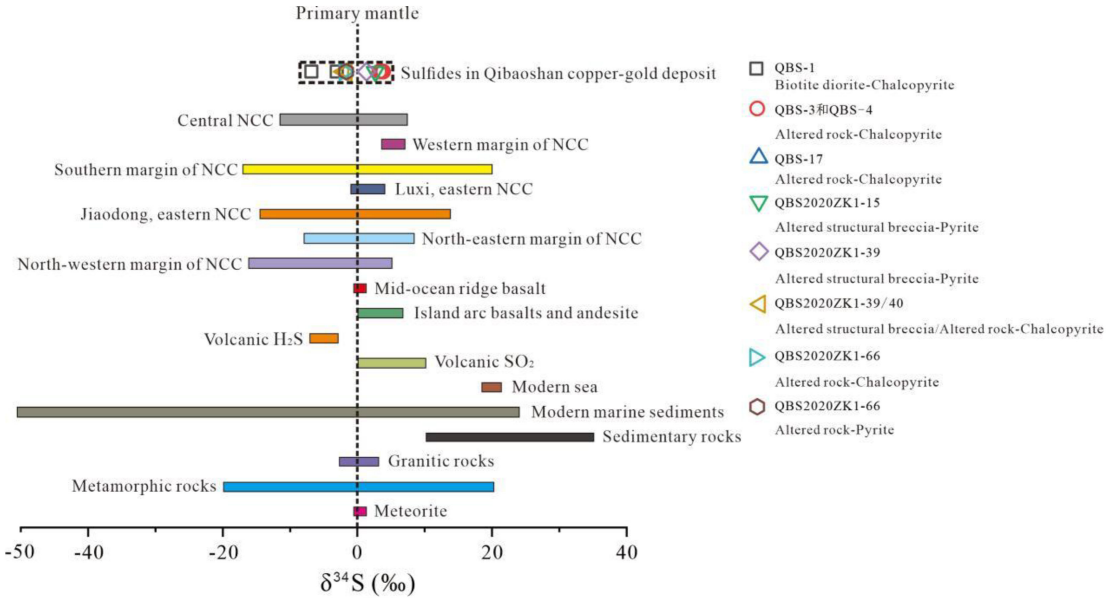


Figure 12. Sulfur isotopic composition of main sulfides in the Qibaoshan Cu–Au polymetallic ore district. (According to [79]).

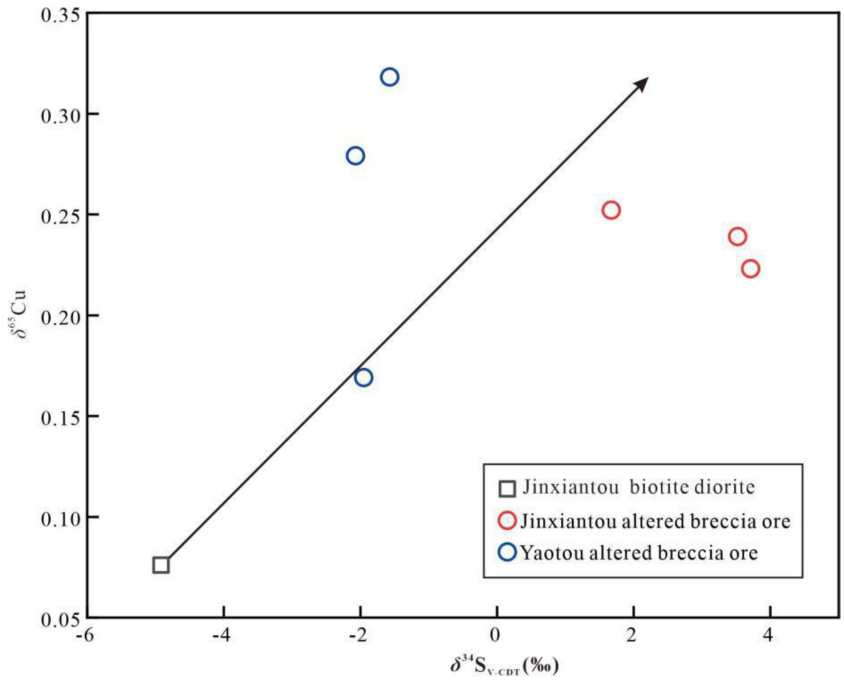


Figure 13. $\delta^{65}Cu$–$\delta^{34}S$ relationship of chalcopyrite in the Qibaoshan Cu–Au polymetallic ore district.

Cu–Au mineralization in the Qibaoshan area is closely related to diorite. Incompatible metallogenic elements (e.g., Au and Cu) are preliminarily enriched in the initial magma melting during the partial melting process. With the cooling and crystallization of quartz diorite porphyrite, supercritical fluid with high salinity is separated from the pluton. In addition, during the phase separation process, the ore-forming elements are more inclined to enter the water-rich fluid phase, and Au, Cu and other ore-forming elements are enriched again. With the decrease of the metallogenic system temperature and the escape of H_2S, CH_4 and other strong reductive fluids, gas transport elements, such as Au and Cu, precipitate in the edge of the porphyry. This corresponds to the mineralization stages of pyrite–quartz and chalcopyrite–chalcocite–bornite–pyrite–quartz. The exhaust of reductive gases, such

as H_2S and CH_4, leads to an increase in oxygen fugacity and pH values. It also results in the crystallization of highly oxidizing minerals, such as specularite, corresponding to the mineralization stage of specularite–pyrite–chalcopyrite–quartz–carbonate. Following this, the oxidization of the ore-forming fluid system is weakened, and the reducibility becomes stronger. The medium low-temperature ore-forming elements, such as Pb, Zn and Cu, precipitate successively, corresponding to the mineralization stages of quartz–polymetallic sulfide and chalcopyrite–pyrite–quartz.

The early Cu–Au ore-forming fluids and the late Pb–Zn ore-forming fluids are superimposed in the Changgou section, and the fracture generated in the process of cryptoexplosion and the fracture developed in the strata provide a channel for the migration of ore-bearing fluids (Figure 14a). All the discovered orebodies are located in the phyllic alteration zone, and the δ^{65}Cu and δ^{34}S values of chalcopyrite in the lower zone tend to decrease (Figure 14b). The decrease in the gas phase and increase in the liquid phase with depth and the decreased δ^{65}Cu values may indicate the existence of concealed pluton or orebodies at depth. Thus, the deep exhibits great prospecting potential. Finally, with the addition of atmospheric precipitation, the temperature and salinity of the fluid system decrease significantly, and the mineralization terminates.

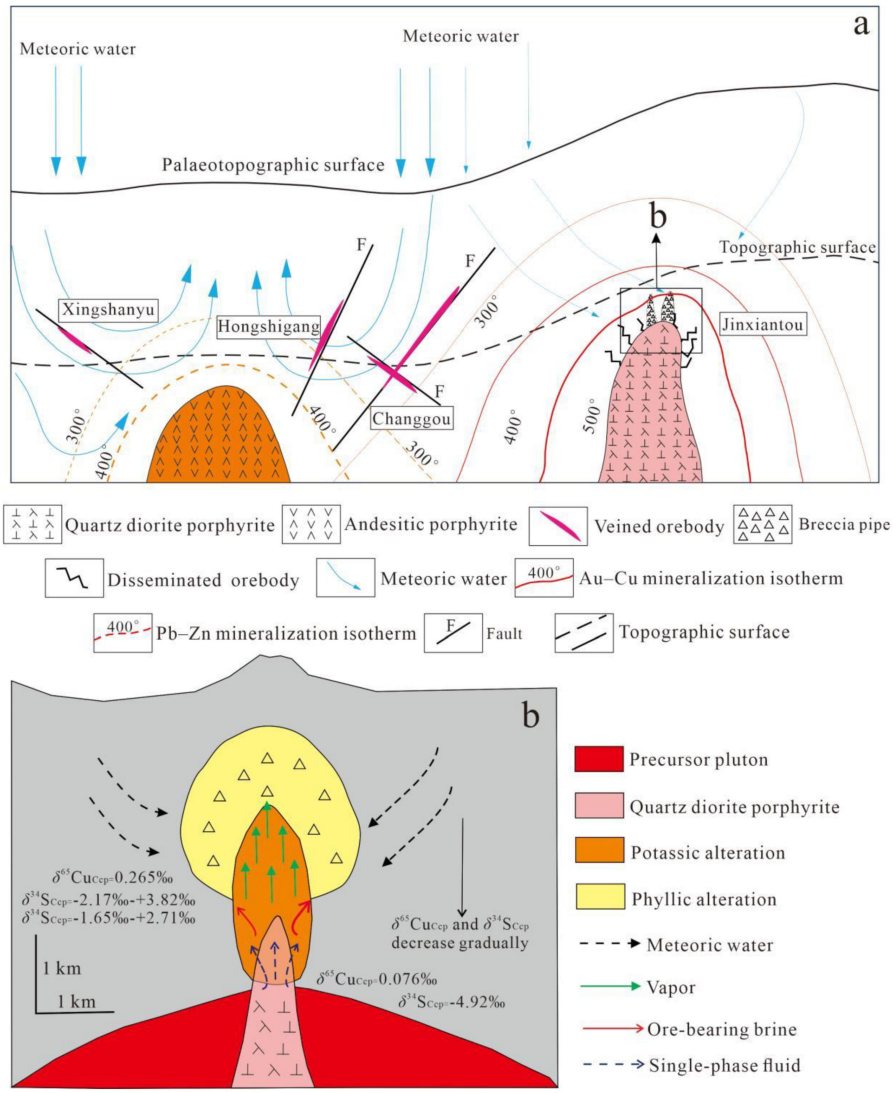


Figure 14. (**a**) Schematic model of mineralization superposition and alteration zoning of Qibaoshan Cu–Au polymetallic ore district (modified from [37,80]). The small box circled in (**a**) is (**b**).

7. Conclusions

Based on the detailed mineralogical observation, Cu and the in situ S isotopic composition of the main sulfides in the Qibaoshan Cu–Au polymetallic ore district suggest that the ore-forming fluid was a mixture between the mantle-derived fluid and the surrounding sedimentary rock.

The results of the Cu and S isotopic compositions of the sulfides in ores decrease with depth, which is likely caused by the upward transport of heavier Cu isotopes. The upper part of the crypto-explosive breccia pipe in the Qibaoshan area may be relatively more gaseous, resulting in the enrichment of δ^{65}Cu.

The decrease in δ^{65}Cu values in the chalcopyrite may indicate the existence of concealed plutons or orebodies at depth, exhibiting prospecting potential in the Qibaoshan area.

Author Contributions: Conceptualization, Y.S.; methodology, Y.Z.; formal analysis, Y.S. and Y.Z.; investigation, Y.Z., W.S., K.G., Q.L., P.W., W.X. and N.C.; resources, X.W.; data curation, Y.S.; writing—original draft preparation, Y.S.; writing—review and editing, Y.Z. and D.L.; project administration, Y.Z. and D.L. All authors have read and agreed to the published version of the manuscript.

Funding: This study was financially supported by the National Natural Science Foundation of China (Grant Nos. 42272104 and 42172094), Natural Science Foundation of Shandong Province (Grant Nos. ZR2019PD005), Geological Exploration Project of Shandong Province (Grant Nos. LKZ (2023) 8).

Conflicts of Interest: The authors declare no conflict of interest.

References

1. Balaram, V.; Satyanarayanan, M. Data Quality in Geochemical Elemental and Isotopic Analysis. *Minerals* **2022**, *12*, 999. [CrossRef]
2. Cook, N.J.; Ciobanu, C.L.; Ehrig, K.; Slattery, A.; Verdugo-Ihl, M.R.; Courtney-Davies, L.; Gao, W. Advances and Opportunities in Ore Mineralogy. *Minerals* **2017**, *7*, 233. [CrossRef]
3. Yuan, H.; Yuan, W.; Bao, Z.; Chen, K.; Huang, F.; Liu, S. Development of two new copper isotope standard solutions and their copper Isotopic compositions. *Geostand. Geoanal. Res.* **2016**, *41*, 77–84. [CrossRef]
4. Moynier, F.; Vance, D.; Fujii, T.; Savage, P. The isotope geochemistry of zinc and copper. *Rev. Mineral. Geochem.* **2017**, *82*, 543–600. [CrossRef]
5. Gou, W.; Li, W.; Ji, J.; Li, W. Zinc Isotope Fractionation during sorption onto Al oxide: Atomic level understanding from EXAFS. *Environ. Sci. Technol.* **2018**, *52*, 9087–9096. [CrossRef]
6. Belshaw, N.; Zhu, X.; Guo, Y.; O'Nions, R. High precision measurement of iron isotopes by plasma source mass spectrometry. *Int. J. Mass Spectrom.* **2000**, *197*, 191–195. [CrossRef]
7. Dauphas, N.; Pourmand, A.; Teng, F. Routine isotopic analysis of iron by HR-MC-ICPMS: How precise and how accurate? *Chem. Geol.* **2009**, *267*, 175–184. [CrossRef]
8. Millet, M.; Baker, J.; Payne, C. Ultra-precise stable Fe isotope measurements by high resolution multiple-collector inductively coupled plasma mass spectrometry with a ^{57}Fe-^{58}Fe double-spike. *Chem Geol.* **2012**, *304*, 18–25. [CrossRef]
9. Sullivan, K.; Layton-Matthews, D.; Leybourne, M.; Kidder, J.; Mester, Z.; Yang, L. Copper Isotopic Analysis in Geological and Biological Reference Materials by MC-ICP-MS. *Geostand. Geoanal. Res.* **2020**, *44*, 349–362. [CrossRef]
10. Wang, Y.; Zhu, X.K. Applications of Cu Isotopes on Studies of Mineral Deposits: A Status Report. *J. Jilin Univ. Earth Sci. Ed.* **2010**, *40*, 739–751. (In Chinese with English Abstract)
11. Zhu, X.K.; Wang, Y.; Yan, B.; Li, J.; Dong, A.G.; Li, Z.H.; Sun, J. Developments of Non-Traditional Stable Isotope Geochemistry. *Bull. Mineral. Petrol. Geochem.* **2013**, *32*, 651–688. (In Chinese with English Abstract)
12. Wang, Z.Z.; Liu, S.A.; Li, D.D.; Lv, Y.W.; Wu, S.; Zhao, Y. A review of progress in copper stable isotope geochemistry. *Earth Sci. Front.* **2015**, *22*, 072–083. (In Chinese with English Abstract)
13. Wang, Y.; Zhu, X.K.; Mao, J.W.; Cheng, Y.B.; Li, Z.H. Preliminary Study on Cu Isotopic Geochemistry Behavior of Dongguashan Porphyry-skarn Deposit, Tongling District. *Acta Geol. Sin.* **2014**, *88*, 2413–2422. (In Chinese with English Abstract)
14. Albarède, F. The stable isotope geochemistry of copper and zinc. *Rev. Mineral. Geochem.* **2004**, *55*, 409–427. [CrossRef]
15. Larson, P.B.; Maher, K.; Ramos, F.C.; Chang, Z.S.; Gaspar, M.; Meinert, L.D. Copper isotope ratios in magmatic and hydrothermal ore-forming environments. *Chem. Geol.* **2003**, *201*, 337–350. [CrossRef]
16. Malitch, K.N.; Latypovc, R.M.; Badanina, I.Y.; Sluzhenikin, S.F. Insights into ore genesis of Ni-Cu-PGE sulfide deposits of the Noril'sk Province (Russia): Evidence from copper and sulfur isotopes. *Lithos* **2014**, *204*, 172–187. [CrossRef]
17. Tang, D.M.; Qin, K.Z.; Su, B.X.; Mao, Y.J.; Evans, N.J.; Niu, Y.J.; Kang, Z. Sulfur and copper isotopic signatures of chalcopyrite at Kalatongke and Baishiquan: Insights into the origin of magmatic Ni-Cu sulfide deposits. *Geochim. Cosmochim. Acta* **2020**, *275*, 209–228. [CrossRef]
18. Graham, S.; Pearson, N.; Jackson, S.; Griffin, W.; O'Reilly, S.Y. Tracing Cu and Fe from source to porphyry: In situ determination of Cu and Fe isotope ratios in sulfides from the Grasberg Cu-Au deposit. *Chem. Geol.* **2004**, *207*, 147–169. [CrossRef]

19. Li, Z.Q.; Yang, Z.M.; Zhu, X.Y.; Hou, Z.Q.; Li, S.Z.; Li, Z.H.; Wang, Y. Cu isotope Composition of Qulong porphyry Cu deposit, Tibet. *Acta Geol. Sinica* **2009**, *83*, 1985–1996. (In Chinese with English Abstract)
20. Mathur, R.; Spencer, T.; Fernando, B.; Brantley, S.; Wilson, M.; Phillips, A.; Munizaga, F.; Maksaev, V.; Vervoort, J.; Hart, G. Exploration potential of Cu isotope fractionation in porphyry copper deposits. *J. Geochem. Explor.* **2009**, *102*, 1–6. [CrossRef]
21. Nie, L.M.; Li, Z.Q.; Fanf, X.J. Cu isotope fractionation during magma evolution process of Qulong porphyry copper deposit, Tibet. *Mineral Depos.* **2012**, *31*, 718–726. (In Chinese with English Abstract)
22. Zheng, Y.C.; Liu, S.A.; Wu, C.D.; Griffin, W.L.; Li, Z.Q.; Xu, B.; Yang, Z.M.; Hou, Z.Q.; O'Reilly, S.Y. Cu isotopes reveal initial Cu enrichment in sources of giant porphyry deposits in a collisional setting. *Geology* **2019**, *47*, 135–138. [CrossRef]
23. Wang, Y. Iron and Copper Isotope Geochemistry of Tongling ore District of the Middle-Lower Yangtze River Valley. Ph.D. Thesis, Chinese Academy of Geological Sciences, Beijing, China, 2011. (In Chinese with English Abstract)
24. Mason, T.F.D.; Weiss, D.J.; Chapman, J.B. Zn and Cu isotopic variability in the Alexandrinka volcanic-hosted massive sulphide (VHMS) ore deposit, Urals, Russia. *Chem. Geol.* **2005**, *221*, 170–187. [CrossRef]
25. Wang, Z.C.; Park, J.W.; Wang, X.; Zou, Z.Q.; Kim, J.; Zhang, P.Y.; Li, M. Evolution of copper isotopes in arc systems: Insights from lavas and molten sulfur in Niuatahi volcano, Tonga rear arc. *Geochim. Cosmochim. Acta* **2019**, *250*, 13–33. [CrossRef]
26. Markl, G.; Yann, L.; Gregor, S. Copper isotopes as monitors of redox processes in hydrothermal mineralization. *Geochim. Cosmochim. Acta* **2006**, *70*, 4215–4228. [CrossRef]
27. Huang, Y.; Sa, R.N.; Zhou, L.; Ou-Yang, X.Q.; Li, X.J.; Shi, G.Y.; Sun, X.M. Fe-Cu isotopic compositions and their indicative significance in Yushui Copper polymetallic deposit, eastern Guangdong Province. *Mineral Depos.* **2014**, *33*, 95–96. (In Chinese with English Abstract)
28. Yang, L.F.; Shi, K.X.; Wang, C.M.; Wu, B.; Du, B.; Chen, J.Y.; Xia, J.S.; Chen, J. Ore genesis of the Jinman copper deposit in the Lanping Basin, Sanjiang Orogen: Constraints by copper and sulfur isotopes. *Acta Petrol. Sinica* **2016**, *32*, 2392–2406. (In Chinese with English Abstract)
29. Ou-Yang, X.C.; Di, Y.J.; Wang, C.M.; Zhang, D.; Yang, Q.; Wu, B.; Wang, Q.; Luo, Z. Genesis of Dongxiang copper deposit in Jiangxi Province: Constraints from copper and sulfur isotopes. *Mineral Depos.* **2017**, *36*, 250–264. (In Chinese with English Abstract)
30. Fan, F.P.; Xiao, H.L.; Chen, L.Z.; Li, H.L.; Liu, J.X.; Deng, Z.L.; Li, S.B.; Lin, G.W.; Zhou, X. Copper Isotope Studies of a Deep Ore Body in the Xinliaodong CopperPolymetallic Deposit, Eastern Guangdong Province. *Rock Miner. Anal.* **2017**, *36*, 420–429. (In Chinese with English Abstract)
31. Wang, Y.; Su, S.G.; Zhang, Q.; Zhou, Q.M.; Zhang, Y.N. Cu-S isotopic characteristics and metallogenic prediction in the ore of Dajing tin and copper polymetallic deposit, Inner Mongolia. *Earth Sci. Front.* **2021**, *29*, 319–328. (In Chinese with English Abstract)
32. Asael, D.; Matthews, A.; Bar-Matthews, M.; Halicz, L. Copper isotope fractionation in sedimentary copper mineralizaion (Timna Valley, Israel). *Chem. Geol.* **2007**, *243*, 238–254. [CrossRef]
33. Asael, D.; Matthews, A.; Oszczepalski, S.; Bar-Matthews, M.; Halicz, L. Fluid speciation controls of low temperature copper isotope fractionation applied to the Kupferschiefer and Timna ore deposits. *Chem. Geol.* **2009**, *262*, 147–158. [CrossRef]
34. Mathur, R.; Ruiz, J.; Titley, S. Cu isotopic fractionation in the supergene environment with and without bacteria. *Geochim. Cosmochim. Acta* **2005**, *69*, 5233–5246. [CrossRef]
35. Maher, K.C.; Larson, P.B. Variation in copper isotope ratios and controls on fractionation in hypogene skarn mineralizaion at Coroccohuayco and Tintaya, Perú. *Econ. Geol.* **2007**, *102*, 225–237. [CrossRef]
36. Kimbll, B.E.; Mathur, R.; Dohnalkova, A.C.; Wall, A.J.; Runkel, R.L.; Brantley, S.L. Copper isotope fractionation in acid mine drainage. *Geochimica Cosmochimica Acta* **2009**, *73*, 1247–1263. [CrossRef]
37. Guo, H.H.; Xia, Y.; Bai, R.X.; Zhang, X.C.; Huang, F. Experiments on Cu-isotope fractionation between chlorine-bearing fluid and silicate magma: Implications for fluid exsolution and porphyry Cu deposits. *Natl. Sci. Rev.* **2020**, *7*, 1319–1330. [CrossRef]
38. Zhu, X.K.; O'Nions, R.K.; Guo, Y.; Belshaw, N.S.; Rickard, D. Determination of natural Cu-isotope variation by plasmasource mass spectrometry: Implications for use as geochemical tracers. *Chem. Geolog.* **2000**, *163*, 139–149. [CrossRef]
39. Rouxel, O.; Fouquet, Y.; Ludden, J.N. Copper Isotope systematics of the lucky strike, rainbow, and logatchev sea-floor hydrothermal field on the mid-Atlantic ridge. *Econ. Geol.* **2004**, *99*, 585–600. [CrossRef]
40. MacDonald, G.D.; Arnold, L.C. Geological and geochemical zoning of the Grasberg Igneous Complex, Irian, Indonesia. *J. Geochem. Explor.* **1994**, *50*, 143–178. [CrossRef]
41. Braxton, D.; Mathur, R. Exploration applications of copper isotopes in the supergene environment: A case study of the Bayugo porphyry copper-gold deposit, southern Philippines. *Econ. Geol.* **2011**, *106*, 1447–1463. [CrossRef]
42. Mathur, R.; Ruiz, J.; Casselman, M.J. Use of Cu isotopes to distinguish primary and secondary Cu mineralizaion in the Cañariaco Norte porphyry copper deposit, Northern Peru. *Miner. Depos.* **2012**, *47*, 755–762. [CrossRef]
43. Mathur, R.; Dendas, M.; Titley, S.; Phillips, A. Patterns in the copper isotope composition of minerals in porphyry copper deposits in southwestern United States. *Econ. Geol.* **2010**, *105*, 1457–1467. [CrossRef]
44. Zhao, H.X.; Li, B.; Zhou, Y.X.; Zhu, Z.Y.; Chen, S.M. Genesis of the giant Zijinshan epithermal Cu-Au deposit, Fujian Province, southeastern China: Cu-He-Ar isotope perspective. *Ore Geology Rev.* **2022**, *148*, 105047. [CrossRef]
45. Wang, Y. Geological characteristics and origin of Qibaoshan gold deposit in Shandong Province. *Geol. Rev.* **1991**, *37*, 327–337. (In Chinese with English Abstract)
46. Yu, G.Y. Metallogenesis and Metallogenic Prognosis of Gold-Copper Polymetallic Deposits in Qibaoshan Orefield, Wulian County, Shandong Province. Ph.D. Thesis, Jilin University, Jilin, China, 2020. (In Chinese with English Abstract)

47. Zhang, L.Y.; Cheng, M.Q. Geochemical characteristics of Qibaoshan Au-Cu deposit Shandong Province and it's genesis. *Contrib. Geol. Miner. Resour. Res.* **1996**, *11*, 18–24. (In Chinese with English Abstract)
48. Tian, N.F.; Zhang, F.; Gao, Z.J.; Yuan, J. Geological Characteristics and Prospecting Direction of Qibaoshan Copper and Polymetallic Mineralization in Wulian County of Shandong Province. *Shandong Land Resour.* **2011**, *27*, 8–11. (In Chinese with English Abstract)
49. Wu, S.S.; Zhang, X.B.; Zhang, Y.; Huang, G.H.; Zhang, T.Z.; Lai, C.K. In-situ trace element and S isotope compositions of sulfides from the Tonggou Cu deposit, Eastern Tianshan Orogen: Implication for ore-forming process. *Ore Geol. Rev.* **2022**, *149*, 105085. [CrossRef]
50. Chugaev, A.V.; Plotinskaya, O.Y.; Dubinina, E.O.; Stepanov, S.Y.; Gareev, B.I.; Batalin, G.A.; Rassokhina, I.V.; Chizhova, J.N.; Bondar, D.; Abramova, V.D. Mixed crustal-mantle source of porphyry Cu-Mo deposits of the Urals: Pyrite trace element geochemistry and Pb-S isotope data. *J. Geochem. Explor.* **2022**, *242*, 107075. [CrossRef]
51. Su, Z.K.; Zhao, X.F.; Wang, C.Y. Trace elements and sulfur isotopic compositions of sulfides in the giant Dahongshan Fe-Cu-(Au-Co) deposit, SW China: Implications for fluid evolution and Co enrichment in IOCG systems. *Ore Geol. Rev.* **2023**, *157*, 105401. [CrossRef]
52. Shi, W.J. The Late Mesozoic Tectonic-magematic Evolution Process in the Yishu Fault Zone and Adjacent Regions, Shandong Province: Implication for Gold Mineralization. Ph.D. Thesis, China University of Geosciences, Beijing, China, 2014. (In Chinese with English Abstract)
53. Qin, K.Z.; Wang, D.B.; Wang, Z.T.; Sun, S. Types, geological background, metallogenic provinces and ore-forming systematics of major copper deposits in eastern China. *Mineral Depos.* **1999**, *18*, 359–371. (In Chinese with English Abstract)
54. Mao, J.W.; Xie, G.Q.; Yuan, S.D.; Liu, P.; Meng, X.Y.; Zhou, Z.H.; Zheng, W. Current research progress and future trends of porphyry-skarn copper and granite-related tin polymetallic deposits in the Circum Pacific metallogenic belts. *Acta Petrol. Sinica* **2018**, *34*, 2501–2517.
55. Zhang, Z.Q.; Zhang, C.J.; Wang, S.J.; Liu, S.C.; Wang, L.M.; Du, S.X.; Song, Z.Y.; Zhang, S.K.; Yang, E.X.; Cheng, G.S.; et al. Views on Classification and Contrast of Tectonic Units in Strata in Shandong Province. *Shandong Land Resour.* **2014**, *30*, 1–23. (In Chinese with English Abstract)
56. Li, X.W.; Shan, W.; Yu, X.F.; Li, D.P.; Xie, Y.H.; Zhang, G.K.; Chi, N.J.; Wang, W.L.; Zhang, Y.; Li, Z.S.; et al. Petrogenesis of Early Cretaceous Qibaoshan alkaline intrusive rocks in the Wulian area and its geological significance. *Earth Sci. Front.* **2022**, *29*, 438–463. (In Chinese with English Abstract)
57. Wang, K.Y.; Wang, X.W.; Zhang, Z.J.; Wang, C.Y.; Yu, Q.; Li, J.F.; Han, Y.Q. Research Report on New Understanding of Copper and Polymetallic ore Mineralization and New Prospecting Methods in Qibaoshan Area, Wulian County, Shandong Province. In *Scientific and Technological Report*; The No. 8 Institute of Geology and Mineral Resources Exploration of Shandong Province: Rizhao, China, 2014. (In Chinese with English Abstract)
58. Wang, X. *The Borehole Histogram from the QBS2020ZK1 Drilling at the Qibaoshan Area, Wulian County. Scientific and Technological Report*; The No. 8 Institute of Geology and Mineral Resources Exploration of Shandong Province: Rizhao, China, 2020. (In Chinese with English Abstract)
59. Liu, S.A.; Teng, F.Z.; Li, S.G.; Wei, G.J.; Ma, J.L.; Li, D.D. Copper and iron isotope fractionation during weathering and pedogenesis: Insights from saprolite profiles. *Geochim. Cosmochim. Acta* **2014**, *146*, 59–75. [CrossRef]
60. Liu, S.A.; Li, D.D.; Li, S.G.; Teng, F.Z.; Ke, S.; Hea, Y.S.; Lu, Y.H. High-precision copper and iron isotope analysis of igneous rock standards by MC-ICP-MS. *J. Anal. Spectrom.* **2014**, *29*, 122–133. [CrossRef]
61. Li, D.D.; Liu, S.A.; Li, S.G. Copper isotope fractionation during adsorption onto kaolinite: Experimental approach and applications. *Chem. Geol.* **2015**, *396*, 74–82. [CrossRef]
62. Maréchal, C.N.; Télouk, P.; Albarède, F. Precise analysis of copper and zinc isotopic compositions by plasma-source mass spectrometry. *Chem. Geol.* **1999**, *156*, 251–273. [CrossRef]
63. Fu, J.; Hu, Z.; Zhang, W.; Yang, L.; Liu, Y.; Li, M.; Zong, K.; Gao, S.; Hu, S. In situ sulfur isotopes (δ34S and δ33S) analyses in sulfides and elemental sulfur using high sensitivity cones combined with the addition of nitrogen by laser ablation MC-ICPMS. *Anal. Chim. Acta* **2016**, *911*, 14–26. [CrossRef]
64. Duan, J.L. Cu and Zn Isotopic Features of Typical Magma-Related Deposit Systems in Tibet and Their Geological Significances. Ph.D. Thesis, China University of Geosciences, Beijing, China, 2018. (In Chinese with English Abstract)
65. Mathur, R.; Munk, L.; Nguyen, M.; Gregogy, M.; Annell, H.; Lang, J. Modern and paleofluid pathways revealed by Cu isotope compositions in surface waters and ores of the Pebble porphyry Cu-Au-Mo deposit, Alaska. *Econ. Geol.* **2013**, *108*, 529–541. [CrossRef]
66. Wu, L.Y.; Hu, R.Z.; Li, X.F.; Liu, S.A.; Tang, Y.W.; Tang, Y.Y. Copper isotopic compositions of the Zijinshan high-sulfidation epithermal Cu-Au deposit, South China: Implications for deposit origin. *Ore Geol. Rev.* **2017**, *83*, 191–199. [CrossRef]
67. Li, W.Q.; Jackson, S.E.; Pearson, N.J.; Graham, S. Copper isotopic zonation in the Northparkes Cu-Au deposit, SE Australia. *Geochim. Cosmochimica Acta* **2010**, *74*, 4078–4096. [CrossRef]
68. Chen, J.; Zhao, Y.; Xue, C.J.; An, W.C.; Guo, X.D. Applications of Cu Isotopes in porphyry deposits. In Proceedings of the 9th National Symposium on Metallogenic Theory and Prospecting Methods, Nanjing, China, 13 December 201; pp. 521–522. (In Chinese with English Abstract)
69. Richter, F.M.; Dauphas, N.; Teng, F.Z. Non-traditional fractionation of non-traditional isotopes: Evaporation, chemical diffusion and Soret diffusion. *Chem. Geol.* **2009**, *258*, 92–103. [CrossRef]

70. Huang, F.; Lundstrom, C.C.; Glessner, J.; Ianno, A.; Boudreau, A.; Li, J.; Ferré, E.C.; Marshak, S.; DeFrates, J. Chemical and isotopic fractio nation of wet andesite in a temperature gradient: Experiments and models suggesting a new mechanism of magma differentiation. *Geochim. Cosmochim. Acta* **2009**, *73*, 729–749. [CrossRef]
71. Çiçek, M.; Oyman, T.; Palmer, M.R. Variation of Cu, Fe, S and Pb isotopes in sulfides from hydrothermal mineralization from the Yenice region in Çanakkale, Biga Peninsula, NW Turkey. *Ore Geol. Rev.* **2021**, *136*, 104255. [CrossRef]
72. Ohmoto, H.; Goldhaber, M.B. Sulfur and Carbon Isotopes. In *Geochemistry of Hydrothermal Ore Deposits*, 3rd ed.; Barnes, H.L., Ed.; John Wiley and Sons: New York, NY, USA, 1997.
73. Bachinski, D.J. Bond Strength and Sulfur Isotopic Fractionation in Coexisting Sulfides: A Reply. *Econ. Geol.* **1969**, *64*, 56–65. [CrossRef]
74. Seal, R.R. Sulfur Isotope Geochemistry of Sulfi de Minerals. *Rev. Mineral Geochem.* **2006**, *61*, 633–677. [CrossRef]
75. Klein, E.L.; Moura, C.A.V.; Harris, C.; Giret, A. Reconnaissance stable isotope (C, O, H, S) study of paleoproterozoic gold deposits of the So Luis Craton and country rocks, Northern Brazil: Implications for gold metallogeny. *Int. Geol. Rev.* **2015**, *11*, 1131–1143.
76. Scherbarth, N.L.; Spry, P.G. Mineralogical, petrological, stable isotope, and fluid inclusion characteristics of the Tuvatu gold-silver Telluride deposit, Fiji: Comparisons with the Emperor Deposit. *Econ. Geol.* **2006**, *101*, 135–158. [CrossRef]
77. Oberthür, T.; Mumm, A.S.; Titley, S.; Vetter, U.; Simon, K.; Amanor, J. Gold Mineralization in the Ashanti Belt of Ghana: Genetic Constraints of the Stable Isotope Geochemis. *Econ. Geol.* **1996**, *91*, 289–301. [CrossRef]
78. Shanks, W.C.P.; Slack, J.F.; Till, A.B.; Thurston, R.; Gemery-Hill, P. Sulfur and oxygen isotopic study of Paleozoic sediment-hosted Zn-Pb(-Ag-Au-Ba-F) deposits and associated hydrothermal alteration zones in the Nome Complex, Seward Peninsula, Alaska. *Geol. Soc. Am.* **2014**, *506*, 235–258.
79. Li, S.R.; Santosh, M. Metallogeny and craton destruction: Records from the North China Craton. *Ore Geol. Rev.* **2014**, *56*, 376–414. [CrossRef]
80. Yu, G.Y.; Li, S.-D.; Wang, Y.C.; Wang, K.Y. Fluid Evolution and Ore Genesis of the Qibaoshan Polymetallic Ore Field, Shandong Province, China: Constraints from Fluid Inclusions and H-O-S Isotopic Compositions. *Minerals* **2019**, *9*, 394. [CrossRef]

Disclaimer/Publisher's Note: The statements, opinions and data contained in all publications are solely those of the individual author(s) and contributor(s) and not of MDPI and/or the editor(s). MDPI and/or the editor(s) disclaim responsibility for any injury to people or property resulting from any ideas, methods, instructions or products referred to in the content.